Gao *et al. Journal of Ovarian Research* (2025) 18:87
https://doi.org/10.1186/s13048-025-01679-2

Journal of Ovarian Research

RESEARCH Open Access

Yijing Decoction improves premature ovarian failure in rats by activating VEGF/VEGFR-2/FAK pathway

Ranran Gao[1†], Yeke Wu[2†], Yuqin Tang[3], Keming Wu[4] and Baojun Guo[1*]

Abstract

Background Premature ovarian failure (POF) is defined as amenorrhea that occurs before the age of 40 when the ovaries weaken or even fail. This disease seriously affects a woman's future health and fertility.

Methods Potential targets of Yijing Decoction (YJD) and POF were predicted by web-based pharmacology-related databases. The POF rat models and human ovarian granulosa cells injury models were induced by triptolide. In addition, the estrous cycle of the rats was monitored by vaginal smear and the ovarian tissue morphology was stained by HE staining. Immunohistochemistry, qRT-PCR and Western blotting were used to evaluate the levels of reproductive and angiogenesis related factors. Moreover, serum levels of the sex hormones and the oxidative stress indicators were measured by ELISA.

Results YJD treatment resulted in the improvement of triptolide-induced abnormal ovarian function by restoring normal estrous cycle, maintaining nearly normal ovarian size, reducing follicular atresia and increasing vascularization. Additionally, YJD treatment normalized the serum levels of P, E2, FSH, LH, AMH, MDA and SOD, while activating the VEGF/VEGFR-2/FAK pathway. However, the VEGF/VEGFR-2/FAK pathway inhibitors reversed these pharmacological effects that YJD exhibited in POF rats. Furthermore, YJD increased the pregnancy rate and the number of live births in POF rats.

Conclusion YJD reduced oxidative stress level, promoted angiogenesis and improved ovarian function in POF rats by activating VEGF/VEGFR-2/FAK pathway. Moreover, YJD improved the intrauterine microenvironment for implantation in POF rats, thereby improving fertility.

Clinical trial number Not applicable.

Keywords Yijing Decoction, Premature ovarian failure, Oxidative stress, Angiogenesis

[†]Ranran Gao and Yeke Wu contributed equally to this work and should be considered co-first authors.

*Correspondence:
Baojun Guo
hnsrmyygbj@zzu.edu.cn
[1]Department of TCM, Henan Provincial People's Hospital, Zhengzhou University, No. 7 Weiwu Road, Jinshui District, Zhengzhou, Henan 450003, China
[2]Department of Stomatology, Hospital of Chengdu University of Traditional Chinese Medicine, Chengdu, Sichuan 610072, China
[3]Department of Clinical Bioinformatics Experimental Center, Henan Provincial People's Hospital, Zhengzhou University, Zhengzhou, Henan 450003, China
[4]Department of Gynaecology, Hospital of Chengdu University of Traditional Chinese Medicine, Chengdu, Sichuan 610072, China

Introduction

Premature ovarian failure (POF) is defined as the cessation of menstruation for a period of at least 3 months before the age of 40, accompanied by elevated levels of follicle stimulating hormone (FSH) exceeding 40 IU·L-1 or menopausal levels, as well as estradiol (E2) levels below 50 $pg{\cdot}mL^{-1}$ on two separate occasions one month apart. This condition is typically characterized by a deficiency of mature follicles, diminished levels of FSH, and reduced ovarian reserve [1]. Common clinical manifestations among affected individuals include irregular menstruation, amenorrhea, and infertility [2]. As quality of life improves and societal factors evolve, the incidence of POF is gradually younger and the incidence rate is increasing year by year, which has attracted more and more attention. The primary treatment options for POF include hormone replacement therapy and assisted reproductive technology, with varying degrees of effectiveness and no definitive cure. These treatments may also lead to adverse reactions such as osteoporosis and cardiovascular diseases [3]. Traditional Chinese medicine offers a promising alternative with its diverse therapeutic applications and potential to mitigate the side effects associated with Western medicine. In recent years, Chinese medicine has gradually taken the advantage in the treatment of POF, thus receiving the attention of the majority of researchers and scholars [4].

The efficacy of Yijing Decoction (YJD) in treating secondary amenorrhea, infertility, and menopausal syndrome has been validated through modern clinical application. Therefore, the renowned herbal medicine YJD was chosen for inclusion in this study. YJD is comprised of eleven herbs, including *Radix Rehmanniae Praeparata*, *Atractylodes macrocephala Koidz*, *Yam*, *Radix Angelica sinensis*, *Jujube seed*, *Radix adenophorae*, *cortex moutan*, *Ginseng Radix*, *Radix Paeoniae Alba*, *Bupleurum*, and *Radix Eucommia ulmoides*. The formula consists of various herbs that have specific functions in nourishing and tonifying different organs in the body. *Radix Rehmanniae Praeparata* nourishes kidney and is accompanied by *Radix Eucommia ulmoides* to tonify kidney [5]. *Radix Angelica sinensis* and *Radix Paeoniae Alba* nourish blood and smooth the liver [6, 7]. *Bupleurum* and *cortex moutan* are included in the formula to detoxify the liver [8]. Additionally, *Yam* and *Atractylodes macrocephala Koidz* are utilized to strengthen the spleen and nourish blood [9]. *Ginseng Radix* and *Radix adenophorae* help to unblock the liver [10], while *Jujube seed* nourishes the heart and calms the mind [11]. Overall, this formula is beneficial for kidney health, spleen strength, heart nourishment, liver regulation, and promotion of blood circulation and menstruation. Clinical trials have demonstrated that the combination of modified YJD and artificial periodic therapy enhances ovarian function in individuals with ovarian reserve dysfunction, renal insufficiency, and liver depletion [12]. YJD positively impacts sex hormone levels, endometrial thickness, and Chinese medicine symptomatology, ultimately leading to improved quality of life for patients. The observed clinical efficacy of this treatment approach is noteworthy.

Ovarian angiogenesis plays a crucial role in follicular development, with vascular endothelial growth factor (VEGF) serving as a key regulator of vascular growth and development [13]. VEGF is primarily produced by granulosa cells, membrane cells, and luteal cells within ovarian tissues. Both VEGF and its receptor VEGFR-2 play significant roles in follicular development, ovulation, and luteal formation [14]. Activation of the VEGF/VEGFR-2 signaling pathway leads to the activation of downstream effectors, including focal adhesion kinase (FAK), which promotes the survival, permeability, and proliferation of ovarian vascular endothelial cells, ultimately aiding in the restoration of ovarian function [15]. Research has demonstrated the significant impact of oxidative stress on ovulation and its role in the progressive accumulation of oxidative damage, which is a key factor in ovarian aging [16]. Patients with POF exhibit elevated levels of reactive oxygen species (ROS), resulting in an imbalance of oxidative processes within the body [17]. Additionally, studies have indicated that heightened expression of VEGF can mitigate oxidative stress within cells [18, 19]. Consequently, investigating the influence of VEGF on ovarian angiogenesis and oxidative stress is essential for enhancing clinical interventions aimed at improving ovarian function.

This study aims to explore the target of action and potential molecular mechanism of YJD in treating POF through network pharmacology analysis. Given the widespread clinical efficacy of YJD, the objective of this investigation is to establish a theoretical framework for the clinical utilization of YJD in POF treatment. By delving into the action mechanism of YJD, this research endeavors to pave the way for future investigations and offer insights to advance the field.

Materials and methods

Screening of potential targets for YJD and POF

YJD compounds were gathered from the Traditional Chinese Medicine Systematic Pharmacology (TCMSP) database and the Encyclopedia of Traditional Chinese Medicine (ETCM), followed by the identification of YJD-related targets from the TCMSP and Swiss Target Prediction databases. A target dataset for POF proteins was established by utilizing the Online Mendelian Inheritance in Humans (OMIM), Gene Cards (GC), and Gene Expression Omnibus (GEO) databases.

Construction and analysis of protein-protein interaction (PPI) network

The common targets of drugs and diseases interactions were entered into the String database for the construction and analysis of PPI networks. The biological species was set as human, and the PPI network was obtained and plotted using Cytoscape 3.7.2 software.

Enrichment analysis of gene ontology (GO) and Kyoto encyclopedia of genes and genomes (KEGG)

GO and KEGG data were enriched and analyzed using FunRich software and the ClusterProfiler software package.

Preparation of YJD

30 g each of *Radix Rehmanniae Praeparata* and *Atractylodes macrocephala Koidz*, 15 g each of *Yam* and *Radix Angelica sinensis*, 9 g each of *Jujube seed* and *Radix adenophorae*, 6 g each of *cortex moutan* and *Ginseng Radix*, and 3 g each of *Radix Paeoniae Alba*, *Bupleurum* and *Radix Eucommia ulmoides* were combined and decocted together for 1 h with water. The resulting filtrate was then extracted and concentrated to create high dose (2.36 g/mL) (H-YJD), medium dose (1.18 g/mL) (M-YJD), and low dose (0.59 g/mL) (L-YJD) based on the amount of raw drug. The solution was refrigerated at 4 °C.

Animals and treatment

Specific pathogen free (SPF) healthy Sprague Dawley (SD) female and male rats (weighing 200–250 g and aged 7 weeks) were purchased from Beijing HFK bioscience CO., Ltd. (Beijing, China). All protocols were authorized by the Ethics Committee of Henan Academy of Traditional Chinese Medicine Animal Experiment Center (SYXK (Yu) 2022-0007). After one week of acclimatization feeding, 60 female rats with normal estrous cycle were selected and randomly divided into six groups. The control group received daily oral gavage of 1 mL/kg physiological saline, while the remaining five groups were administered 400 μg/kg triptolide (TP) via oral gavage daily for a duration of 8 weeks. Following 2 weeks of continuous TP administration, rats in the treatment group respectively received low (5.9 g/kg), medium (11.8 g/kg) and high (23.6 g/kg) doses of YJD via oral gavage based on the amount of raw drug, and divided into TP + L-YJD group, TP + M-YJD group and TP + H-YJD group [20]. The rats in TP + DHEA group were given a daily oral gavage dehydroepiandrosterone (DHEA) at dose of 13.5 mg/kg for 8 weeks [21]. Saline (1 mL/kg per day) was administered via oral gavage to rats in both the TP and control groups, and the first day of drug administration was recorded as D1. In addition, rats were continuously monitored for vaginal smears, ovaries, and body weight for 56 days from D1 onwards. All the diestrus females were sacrificed after the model was established, and the serum and ovaries of the diestrus females were obtained for studying the mechanism of action of YJD on POF rats in vivo.

Female rats in estrus after modeling were utilized to evaluate the effect of YJD on female fertility. Male rats were individually housed in cages for mating purposes. Female rats that exhibited estrus, as determined by counting estrous cycles in the preceding experimental phase, were paired with males in a 1:1 ratio. The presence of a vaginal plug was an indicator of successful mating, with the day of plug detection recorded as the first day of pregnancy (P1). At P10, three female rats from each group were euthanized to assess the number of implanted embryos, as well as to collect blood and ovaries for sex hormone level analysis during pregnancy. The remaining pregnant female rats in each group were kept until natural delivery and the number of pups born alive/dead and litter weight were recorded. The pregnancy rate, average number of embryos implanted, number of live births and neonatal weight of rats in each group were counted.

Hematoxylin-eosin staining (HE)

The tissue was dehydrated with ethanol and xylene, followed by paraffin embedding. After the tissue was cut into wax slices with a thickness of 5 μm, the sections were dried, deparaffinized and rinsed with distilled water. Subsequently, the sections were stained with hematoxylin, rinsed with flowing water, and then stained with eosin. After being dehydrated and sealed, the prepared sections were examined under a light microscope. The histomorphology of the rat ovary was observed and the number of follicular cells at all levels (primordial follicle, primary follicle, secondary follicle, sinus follicle, atretic follicle) was statistically analyzed. Hematoxylin and eosin were purchased from Wuhan Xavier Biotechnology Co., LTD (Wuhan, Hubei, China).

Immunohistochemistry (IHC)

The sections were rapidly cooled with cold water after immersion in an antigen retrieval solution, followed by washing twice with phosphate-buffered saline (PBS). The washed sections were then treated with an endogenous peroxidase blocking agent and incubated in darkness at room temperature. Subsequently, primary antibodies were applied to the sections at 37℃ for 30 min, followed by incubation with enzyme-labeled goat anti-mouse/rabbit IgG secondary antibody (1:100, PV-6000; Beijing Zhongshan Jinqiao Biotechnology Co. LTD, Beijing, China) at 37℃ for 20 min. Color development was achieved using 3,3'-diaminobenzidine (DAB) (Wuhan Xavier Biotechnology Co., LTD, Wuhan, Hubei, China), followed by staining with hematoxylin and final dehydration to seal the sections. The prepared sections were

placed under a light microscope and the images were captured. Primary antibodies were used as follows: anti-Platelet endothelial cell adhesion molecule-1 (CD31) antibody (1:200, A01513-3), anti-α-Smooth muscle actin (α-SMA) antibody (1:200, BM3902), anti-VEGF antibody (1:200, BA0407), anti-VEGFR-2 antibody (1:200, A00901-3), anti-FAK antibody (1:200, BM4303). These primary antibodies were purchased from Boster Biological Technology (Pleasanton, CA, USA).

Immunofluorescence (IF)

The deparaffinization and antigen retrieval of tissue sections were performed as described in immunohistochemical procedures. The antigen-repaired sections were subjected to incubation with primary antibodies against mouse vasa homologue (MVH) (1:200, BA2882; Boster Biological Technology, Pleasanton, CA, USA) and octamer-binding transcription factor 4 (Oct4) (1:200, A00174; Boster Biological Technology, Pleasanton, CA, USA) overnight at 4 °C. Following primary antibody incubation, the tissues underwent incubation with Cy3-labeled goat anti-rabbit IgG secondary antibody (1:100, GB21303; Wuhan Xavier Biotechnology Co., LTD, Wuhan, Hubei, China) for 1 h at room temperature in the absence of light. Subsequently, the sections were washed with PBS and incubated with DAPI for 15 min. An anti-fluorescence quencher was then applied, and the slices were sealed and dried. All procedures were performed in darkness after the introduction of secondary antibodies. The tissue sections were placed under an inverted confocal microscope for tissue scanning, and the original data images were reconstructed and simulated in three dimensions by using Imaris software and Image J software.

Enzyme-linked immunosorbent assay (ELISA)

Serum levels of the hormones progesterone (P), E2, FSH, luteinizing hormone (LH), and anti-mullerian hormone (AMH), and the oxidative stress indicators malondialdehyde (MDA) and superoxide dismutase (SOD) were measured by using ELISA kits. And the experiments were performed according to the instructions for the kits. Rat P ELISA kit, rat E2 ELISA kit, rat FSH ELISA kit, rat LH ELISA kit, rat AMH ELISA kit, and rat MDA ELISA kit were purchased from Elabscience Biotechnology Co., LTD (Wuhan, Hubei, China). The rat SOD ELISA kit was purchased from Jianglai Biotechnology Co., LTD (Shanghai, China).

Quantitative real-time PCR (qRT-PCR)

Total RNA was extracted by adding TRIzol reagent (Invitrogen, Thermo Fisher Scientific Inc., Waltham, MA, USA) in each group. Subsequently, the extracted total RNA was reversely transcribed into cDNA according to the instructions of PrimeScript RT reagent Kit (Takara, Tokyo, Japan), and then the cDNA was amplified. The primers were designed by Primer-BLAST software and synthesized by Thermo Fisher Scientific (Waltham, MA, USA), and the primer sequences and product lengths are shown in Table 1. The relative expression of VEGF, VEGFR-2, and FAK mRNA was calculated using the $2^{-\Delta\Delta CT}$ method with β-actin as an internal reference.

Western blotting (WB)

The total protein extracted was quantified for protein concentration utilizing the bicinchoninic acid (BCA) kit (Biosharp, Guangzhou, Guangdong, China). Following a 5-minute heating and denaturation process, a portion of the denatured protein samples underwent electrophoresis on sodium dodecyl sulfate (SDS) polyacrylamide gel. Subsequently, the proteins were transferred from the gel to polyvinylidene fluoride (PVDF) membrane and blocked with 5% skimmed milk powder for a duration of 1 h at ambient temperature. The membrane was then subjected to incubation with primary antibodies for VEGF(1:1,000, BA0407; Boster, Pleasanton, CA, USA), VEGFR-2 (1:1,000, BM4256; Boster, Pleasanton, CA, USA), FAK(1:1,000, PB0662; Boster, Pleasanton, CA, USA), p-VEGFR-2(1:1,000, AP0382; ABclonal Technology Co., LTD, Wuhan, Hubei, China), p-FAK(1:1,000, AF1960; Beyotime Biotechnology, Shanghai, China), B-cell lymphoma-2 (Bcl-2) (1:1,000, ab182858; Abcam, Cambridge, MA, USA), pro-Caspase-3(1:1,000, ab32499; Abcam, Cambridge, MA, USA), Caspase-3 (1:1,000, ab32351; Abcam, Cambridge, MA, USA), apoptosis-inducing factor (AIF) (1:1,000, ab137725; Abcam, Cambridge, MA, USA), and β-actin (1:1,000, ab8227; Abcam,

Table 1 List of primers used in the study

Number	Gene	Primer sequence	Primer length
1	β-actin	Forward 5′-CTGAGAGGGAAATCGTGCGT-3′	
		Reverse 5′-CCACAGGATCCATACCCAAGA-3′	150 bp
2	VEGF	Forward 5′-GAGCGTTCACTGTGAGCCTTGT-3′	
		Reverse 5′-TTAACTCAAGCTGCCTCGCCT-3′	122 bp
3	VEGFR-2	Forward 5′-TTGGCAAATACAACCCTTCAGAT-3′	
		Reverse 5′-GCAGAAGATACTGTCACCACCG-3′	132 bp
4	FAK	Forward 5′-CAACCACCTGGGCCAGTATTATC-3′	
		Reverse 5′-CCATAGCAGGCCACATGCTTTA-3′	138 bp

Cambridge, MA, USA) overnight at 4 °C. After washing three times with TBST buffer, the horseradish peroxidase (HRP)-labeled goat anti-rabbit IgG secondary antibody (1:5000, BM3894; Boster, Pleasanton, CA, USA) was introduced and the membrane was incubated for 1 h at room temperature. The relative expression of the target protein was analyzed by Image J v1.8.0 software.

Cell culture and treatment

Human ovarian granulosa (KGN) cells were purchased from the Procell life science & technology Co., LTD (Wuhan, Hubei, China). The cells were cultured in Dulbecco's Modified Eagle Medium/Nutrient Mixture F-12 (DMEM/F12) medium (Gibco, Thermo Fisher Scientific Inc., Waltham, MA, USA) supplemented with 10% fetal bovine serum (Gibco, Thermo Fisher Scientific Inc., Waltham, MA, USA) and 1% penicillin-streptomycin (Sangon-Biotech, Shanghai, China). The culture condition was 37℃ and 5% CO_2. After the KGN cells were adhered to the plate for 24 h, the supernatant was discarded. In order to establish a cell model of ovarian damage, KGN cells were treated with 200 μL of TP at a concentration of 100 nM and incubated for 12 h. The KGN cells were exposed to medicated serum at varying concentrations (0%, 5%, 10%, 15%, and 20%) to determine the optimal concentration of YJD in subsequent experiments. Subsequently, the effect of YJD on the cell model was further investigated by treating TP-induced KGN cells with 5%, 10%, and 15% medicated serum. Additionally, the potential involvement of the VEGF/VEGFR-2/FAK signaling pathway in the therapeutic effects of YJD on POF was explored by adding VEGF inhibitor (Avastin), VEGFR-2 inhibitor (SU5408) and FAK inhibitor (Y15) to TP-induced KGN cells supplemented with 15% medicated serum. After drug treatment, the culture was continued for 24 h.

Cell counting kit-8 (CCK-8) assay

A medicated serum was generated through continuous gavage of SD rats with M-YJD. Various concentrations (0%, 5%, 10%, 15%, and 20%) of medicated serum were applied to KGN cells, and their inhibition ratio was assessed using CCK-8 kit (Yeasen Biotechnology Co., LTD, Shanghai, China). Subsequently, 5%, 10%, and 15% medicated serum were employed to treat TP-induced KGN cells for cell viability assessment and subsequent experiments.

Annexin V-fluorescein isothiocyanate (Annexin V-FITC) apoptosis assay

Cell samples from each experimental group were collected and processed to achieve a concentration of 10^5 cells per milliliter in a suspension. The cells were subsequently washed with phosphate-buffered saline (PBS), centrifuged, and the resulting supernatant was removed before resuspending the cells. Following this, the cells were treated with Annexin V-FITC/propidium iodide (PI) kit (Invitrogen, Thermo Fisher Scientific Inc., Waltham, MA, USA) according to the instructions of the kit, and then allowed to incubate at room temperature for 15 min. Finally, the samples were analyzed using flow cytometry.

Statistical analysis

Each assay was performed for 3 times. Data were analyzed by GraphPad Prism 8.0 (La Jolla, CA, USA) and expressed as mean ± standard deviation. Two-tailed Student's t test were used for comparing two variables. One-way ANOVA test was used for multiple variable comparison. $P<0.05$ was considered as a significant difference.

Results

Angiogenesis and oxidative stress might be involved in treatment of YJD on POF by bioinformatics analysis

The targets corresponding to the active ingredients of YJD were obtained from TCMSP, which yielded overlapping 171 targets upon intersecting with POF disease targets from Gene card (Fig. 1A). VEGFA was observed in a network map of the relationships between these 171 targets and the active ingredients of 11 herbs in YJD (Fig. 1B). Additionally, VEGFA and VEGFR were overlapping target genes of POF and YJD and had relatively strong interaction with other target genes by the PPI network diagram (Fig. 2A). The biological processes (BP), cell components (CC) and molecular functions (MF) involved in overlapping target genes were analyzed by GO enrichment analysis (Fig. 2B). Among them, overlapping target genes enrichment was observed in response to oxidative stress, response to decreased oxygen levels and response to ROS in the top 10 BP entries. Furthermore, KEGG enrichment analysis was utilized to cluster the pathway functions on the overlapping target genes. Chemical carcinogenic ROS and VEGF signaling pathways existed in the top 20 pathways enriched by overlapping target genes of YJD and POF (Fig. 2C). Therefore, these findings indicated that oxidative stress and angiogenesis might be involved in treatment of YJD on POF.

YJD reduced oxidative stress, enhanced angiogenesis and improved ovarian function in POF rats

Vaginal cell smears in rats showed different cell compositions during different stages of the estrous cycle: proestrus had mostly nuclear epithelial cells, estrus had patches of keratinized cells, metoestrus had equal proportions of keratinized cells and leukocytes, and diestrus had mostly leukocytes with some mucus (Fig. 3A). The results of vaginal cell smears implied that the estrous cycle of the TP model group was disturbed, which

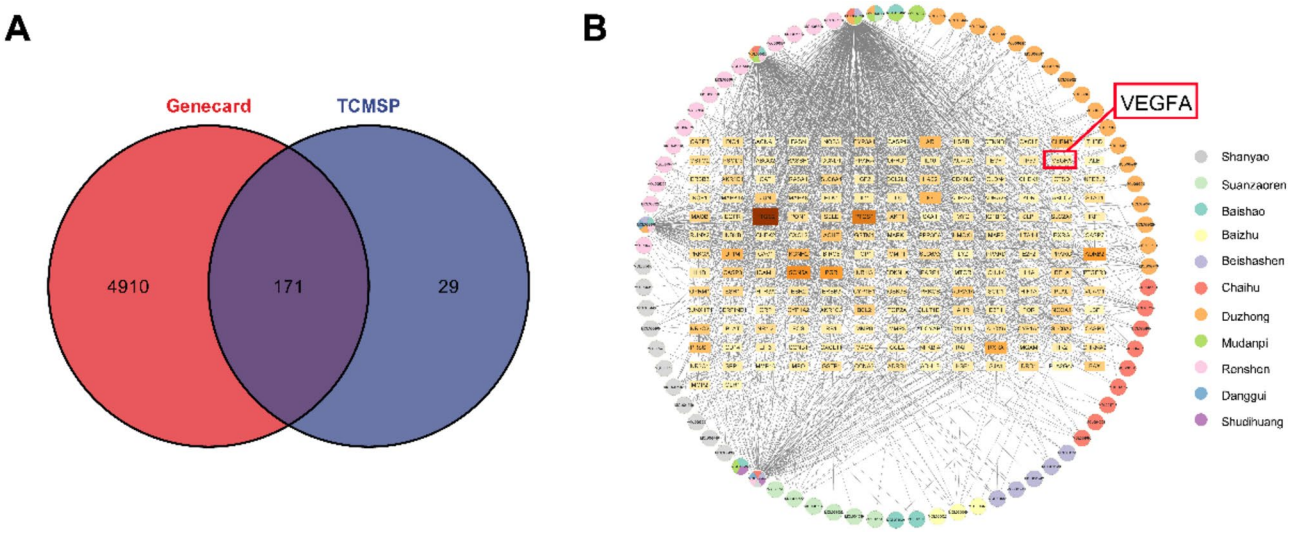

Fig. 1 Bioinformatics analysis of the correlation between YJD and POF. (**A**) Venn diagram of POF target genes established by Gene Card and YJD active ingredients target genes obtained from TCMSP. (**B**) The network map of the overlapping target genes and the 11 herbs active components of YJD

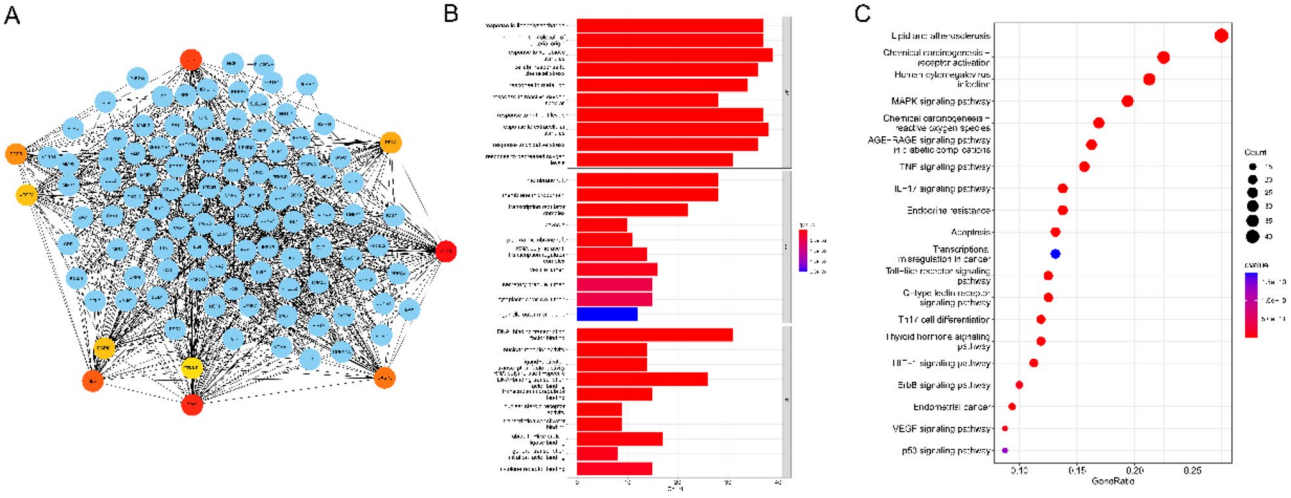

Fig. 2 Functional and pathway enrichment analysis of the overlapping target genes of YJD and POF. (**A**) PPI network analysis was utilized to observed the interaction between these overlapping targets. (**B**) Bar charts of GO enrichment analysis of YJD and POF shared targets of action. (**C**) Bubble plots of KEGG enrichment analysis of YJD and POF shared targets of action

returned to normal after YJD or DHEA treatment (Fig. 3B-C). Additionally, YJD or DHEA therapy restored the weight loss induced by TP-induced POF in rats (Fig. 3D). The decrease in ovarian wet weight and ovarian index in the POF rat models was improved by YJD or DHEA treatment (Fig. 3E-F). The smaller ovaries with fewer follicles and disorganized granulosa cells were observed in TP group by HE staining. YJD or DHEA caused normalized ovarian volume and an increased number of follicles (Fig. 3G). Quantification of follicles at various developmental stages through HE staining indicated that the model group had fewer follicles at all levels compared to the normal group, with an increase in atretic follicles. Addition of YJD or DHEA resulted in the normalization of follicle counts across all stages, with the most pronounced therapeutic effect observed with M-YJD treatment (Fig. 3H-L). Thus, YJD exhibited improvement in ovarian function in POF rats, among which M-YJD had the strongest effect.

The results of IHC assay presented that decreased microvessel density were found in TP model group. Treatment with either YJD or DHEA led to a marked increase in CD31 and α-SMA positive staining in the follicles and corpus luteum and microvessel density of POF rats (Fig. 4A-C). P, E2, and AMH levels in the TP model group decreased while FSH and LH levels increased compared to the control group by ELISA assays. After treatment with YJD or DHEA, an increase of P, E2, and AMH

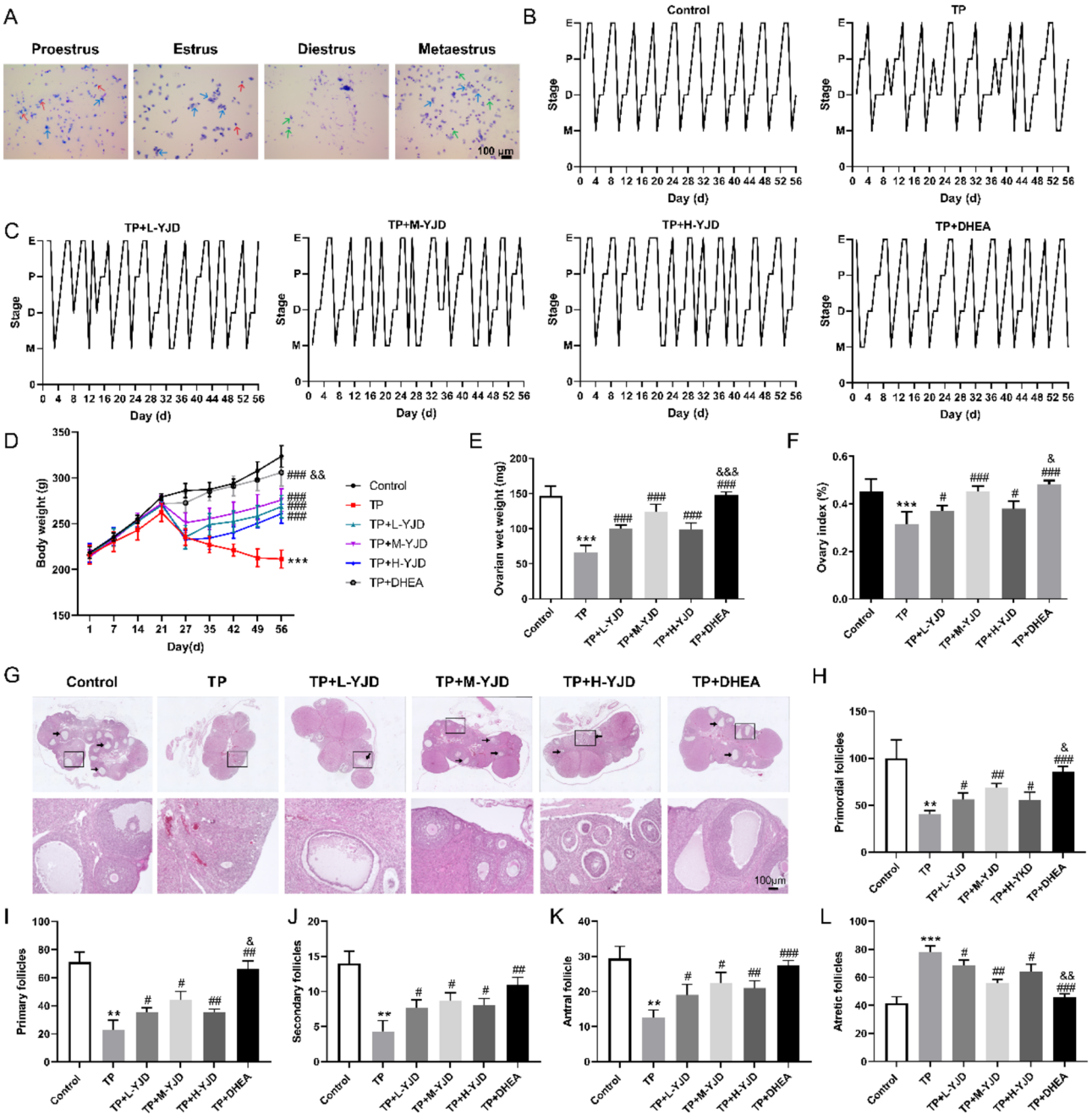

Fig. 3 YJD affected ovarian function in POF rats. (**A**) Vaginal exfoliated cell smears were used to observe the morphological changes of cells at various stages of the estrous cycle of rats; Red arrows point to nucleated epithelial cells; Blue arrows point to keratinized cells; Green arrows point to white blood cells; (Note: The estrous cycle of rats is 4 ~ 5 days. The morphological changes in vaginal cytological smears of the rat estrous cycle were categorized as proestrus, estrus, metoestrus, and diestrus. After rats were modeled with TP, L-YJD, M-YJD and H-YJD as well as DHEA positive controls were added. (**B**-**C**) From the beginning of drug administration (D1), the estrous cycle of each rat was examined daily by vaginal smear, and the estrous cycles of the different groups were counted. (**D**) Since the beginning of drug administration (D1), the dynamic changes in body weight of rats in each group were counted. (**E**) Bilateral intact ovary weights were weighed. (**F**) Ovarian index was calculated (ovarian index = bilateral ovarian wet weight (mg)/body weight (g) × 100%). (**G**) Ovarian tissue morphology was observed by HE staining and light microscopy; Black arrows point to the follicle. (**H**–**L**) The number of follicles at each level in HE staining was counted. (Primordial follicle: oocyte surrounded by a layer of flattened granulosa cells; Primary follicle: oocyte surrounded by a layer of cuboidal granulosa cells; Secondary follicle: oocyte with two or more layers of cuboidal granulosa cells, and without follicular sinus; Sinus follicle: follicular sinus cavity is large, with a pronounced cumulus; Atretic follicle: follicular wall collapsed with damage to the structure of the oocyte, and the loss of hyaline zone.) $^{*}P<0.05$, $^{**}P<0.01$, $^{***}P<0.001$ vs. Control; $^{\#}P<0.05$, $^{\#\#}P<0.01$, $^{\#\#\#}P<0.001$ vs. TP; $^{\&}P<0.05$, $^{\&\&}P<0.01$, $^{\&\&\&}P<0.001$ vs. TP + M-YJD

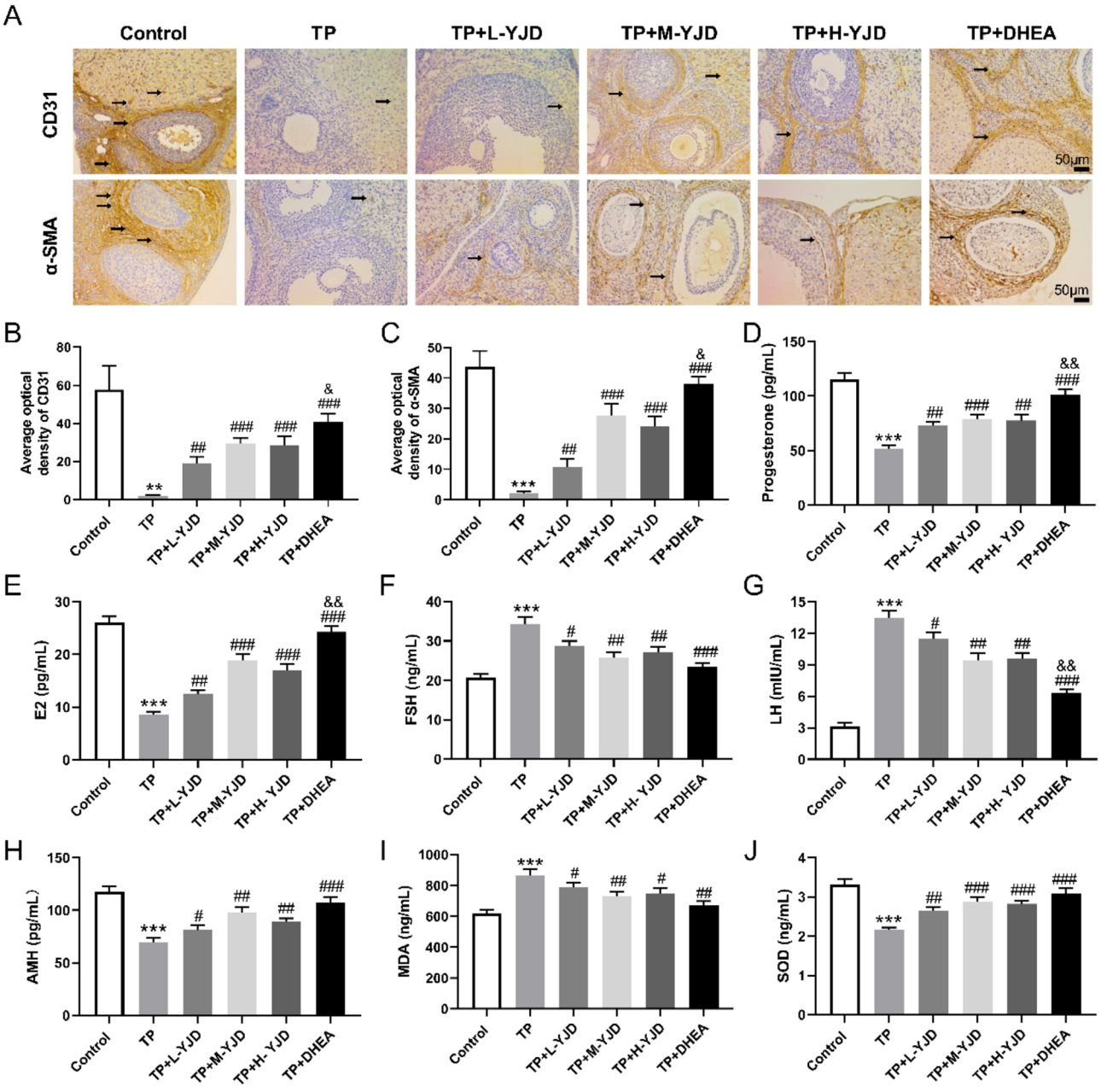

Fig. 4 YJD affected angiogenesis and oxidative stress in POF rats. (**A**) IHC was performed to detect the expression of CD31 and α-SMA, which is located around growing follicles in the ovaries; Black arrows point to areas of positive staining. (**B**) Average optical density of CD31. (**C**) The average optical density of α-SMA. (**D**–**H**) Serum levels of the hormones P, E2, FSH, LH, and AMH were examined by ELISA. (**I**–**J**) Serum levels of indicators of oxidative stress, MDA and SOD, were assessed by ELISA. $^{***}P < 0.001$ vs. Control; $^{\#}P < 0.05$, $^{\#\#}P < 0.01$, $^{\#\#\#}P < 0.001$ vs. TP; $^{\&}P < 0.05$, $^{\&\&}P < 0.01$, $^{\&\&\&}P < 0.001$ vs. TP + M-YJD

levels and a decrease of FSH and LH levels were observed (Fig. 4D-H). MDA and SOD levels also normalized after treatment with YJD or DHEA (Fig. 4I-J).

As a result, YJD demonstrated efficacy in improving TP-induced ovarian dysfunction by restoring a normal estrous cycle, leading to near-normal ovarian size, and decreasing follicular atresia. Additionally, YJD treatment caused an increase in ovarian angiogenesis and a decrease in oxidative stress in POF rats.

YJD activated VEGF/VEGFR-2/FAK signaling pathway in POF rats

IF analysis of germ cell-specific markers MVH and Oct4 demonstrated a significant decrease in expression levels in the TP group compared to the control group. Conversely, expression levels of both MVH and Oct4 were significantly elevated in the L-YJD, M-YJD, and H-YJD groups compared to the TP group, with the best therapeutic effect in M-YJD treatment. Furthermore, the

DHEA group also exhibited a significant increase in expression levels (Fig. 5A-B). Additionally, the qRT-PCR and IHC results indicated that YJD led to a significant increase in the expression of VEGF, VEGFR-2, and FAK in POF rats (Fig. 5C-D). The results of WB assay further revealed that the expression of p-VEGFR-2 and p-FAK also was increased after YJD treatment in TP-induced POF rats (Fig. 5E-F). Hence, YJD resulted in the activation of the VEGF/VEGFR-2/FAK signaling pathway in rats with POF.

YJD improved TP-induced KGN cell injury and activated VEGF/VEGFR-2/FAK pathway in vitro

CCK-8 method was employed to screen out 5%, 10% and 15% YJD medicated serum for the treatment on TP-induced KGN cells in subsequent experiments by assessing the cell inhibition ratio of various concentrations of YJD medicated serum on KGN cells (Fig. 6A). Cells viability decreased in TP-induced KGN cells but increased with the increase of YJD concentration (Fig. 6B). Levels of P, E2, and AMH were significantly reduced in the TP group, while FSH and LH levels were elevated. The addition of YJD gradually restored all sex hormone levels to normal by ELISA detection (Fig. 6C-G). In addition, qRT-PCR results exhibited decreased expression of VEGF, VEGFR-2, and FAK in TP group, but increased their expression with YJD (Fig. 6H). WB confirmed that phosphorylation levels of angiogenesis markers were gradually increased with the increase of YJD concentration (Fig. 6I-J). Moreover, the results of Annexin V-FITC flow cytometry showed that TP-induced apoptosis of KGN cells was gradually reduced with the increase of YJD treatment concentration (Fig. 6K). With the increase of YJD treatment concentration, the expression of pro-Caspase-3, Caspase-3 and AIF was gradually decreased, while the expression of anti-apoptotic factor Bcl-2 was increased as confirmed by WB (Fig. 6L). Therefore, YJD induced the activation of VEGF/VEGFR-2/FAK pathway and the inhibition of apoptosis in TP-induced KGN cells.

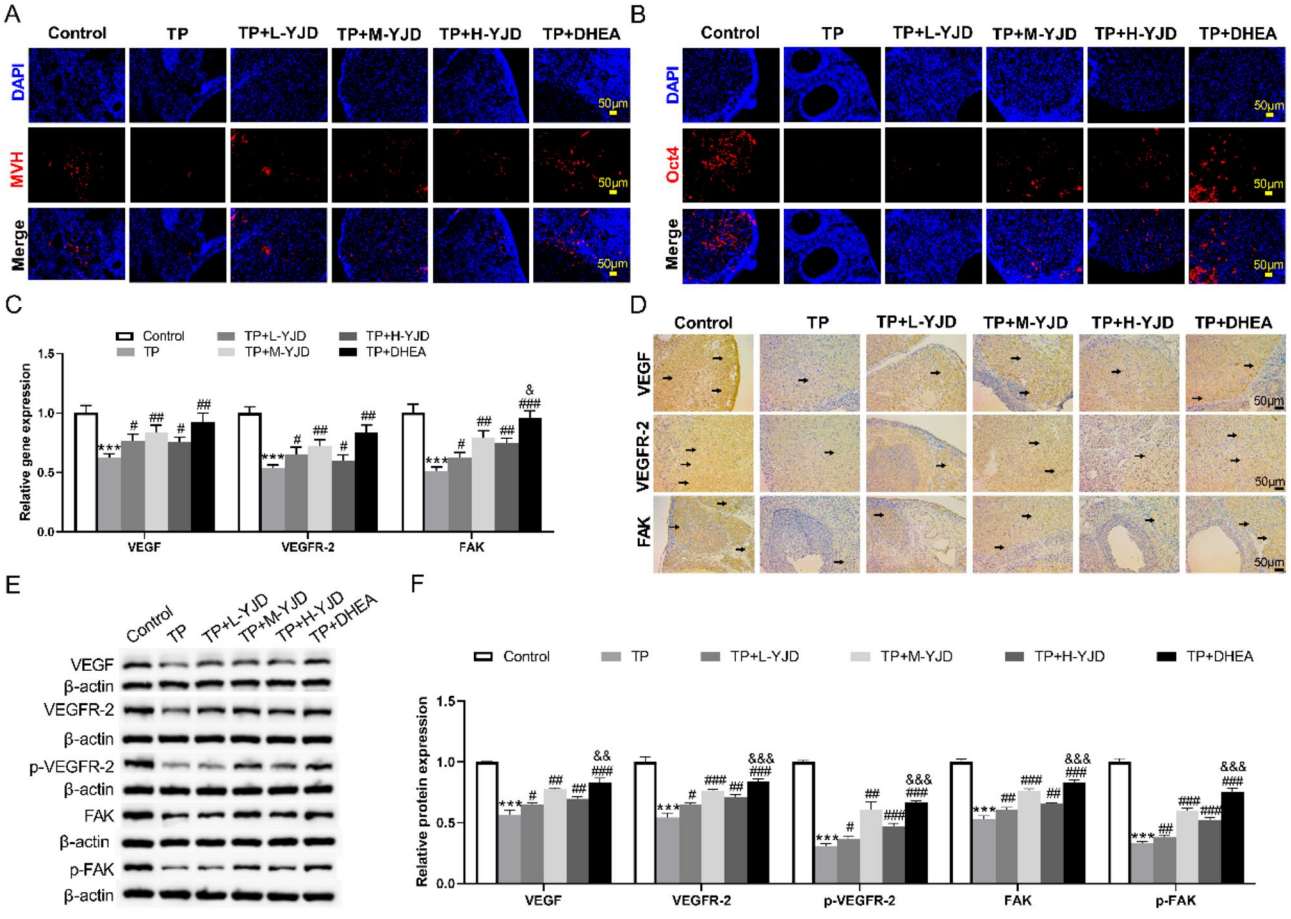

Fig. 5 YJD affected the VEGF/VEGFR-2/FAK pathway in vivo. (**A**–**B**) Germ cell markers MVH and Oct4 were detected by IF. (**C**) The expression of VEGF, VEGFR-2, and FAK was detected by qRT-PCR. (**D**) VEGF, VEGFR-2, FAK expression in the ovaries was examined by IHC; Black arrows point to areas of positive staining. (**E**-**F**) The expression of VEGF, VEGFR-2, FAK, p-VEGFR-2 and p-FAK were assessed by WB. $^{**}P<0.01$, $^{***}P<0.001$ vs. Control; $^{\#}P<0.05$, $^{\#\#}P<0.01$, $^{\#\#\#}P<0.001$ vs. TP; $^{\&}P<0.05$, $^{\&\&}P<0.01$ vs. TP + M-YJD

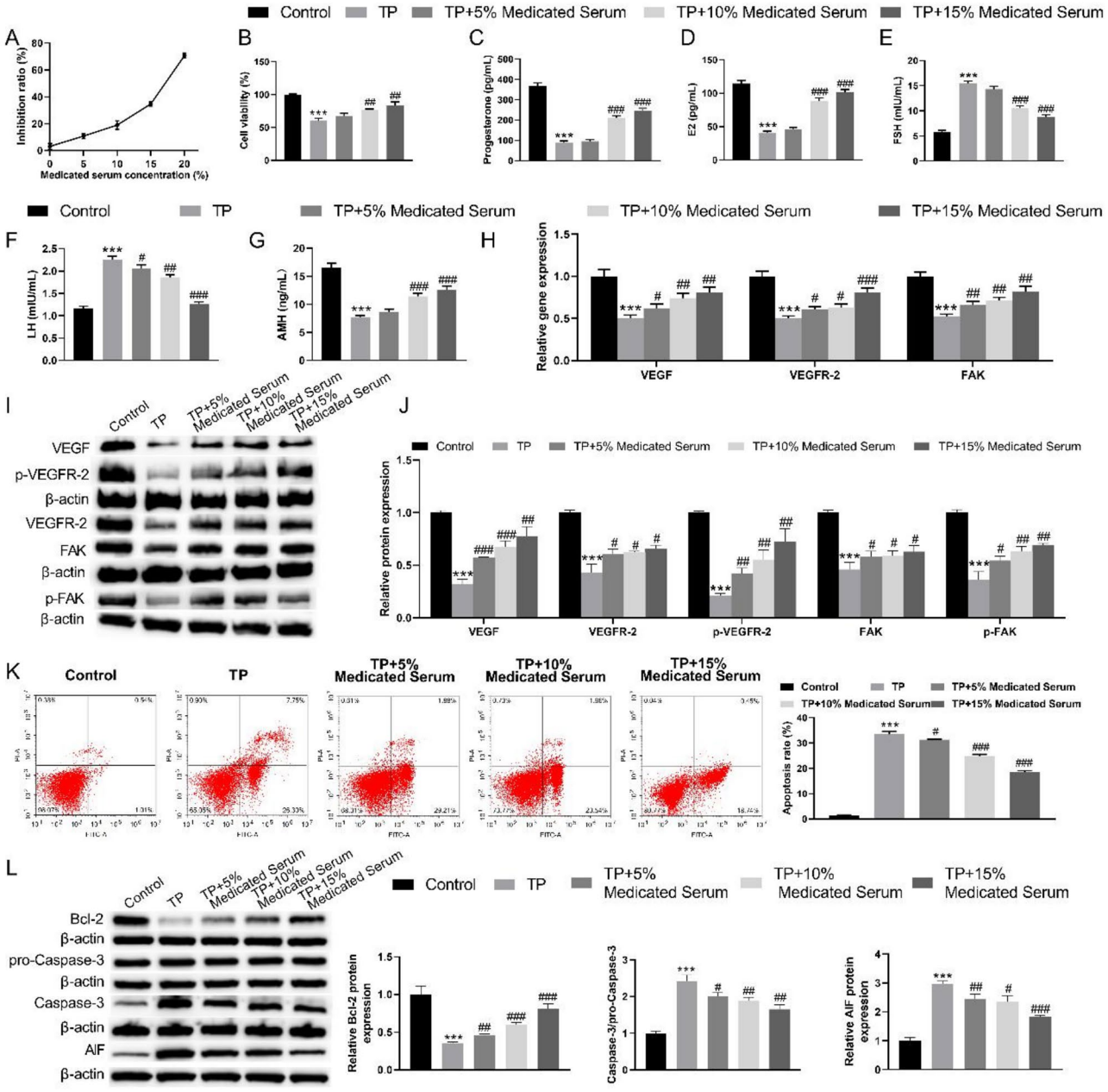

Fig. 6 YJD affected the VEGF/VEGFR-2/FAK pathway and KGN cell injury in vitro. (**A**) Screening of YJD for medicated serum concentrations utilized the CCK-8 assay. (**B**) The cell viability of each group was measured by CCK-8. (**C**–**G**) Serum levels of the hormones P, E2, FSH, LH, and AMH were examined by ELISA. (**H**) The expression of VEGF, VEGFR-2, and FAK was detected by qRT-PCR. (**I**-**J**) The expression of VEGF, VEGFR-2, FAK, p-VEGFR-2 and p-FAK were assessed by WB. (**K**) Apoptosis index was detected by Annexin V-FITC flow cytometry. (**L**) The expression of Bcl-2, pro-Caspase-3, Caspase-3 and AIF were assessed by WB. $^{**}P < 0.01$, $^{***}P < 0.001$ vs. Control; $^{\#}P < 0.05$, $^{\#\#}P < 0.01$, $^{\#\#\#}P < 0.001$ vs. TP

YJD improved POF and reduced oxidative stress by activating VEGF/VEGFR-2/FAK signaling pathway in vitro

To explore whether YJD improved POF by regulating VEGF/VEGFR-2/FAK signaling pathway, TP-induced KGN cells treated with 15% medicated serum were supplemented with VEGF inhibitor, VEGFR-2 inhibitor, and FAK inhibitor, respectively. Compared with the TP + 15% medicated serum treatment group, the addition of angiogenesis marker inhibitors caused a reduction in the levels of P, E2 and AMH and an increase in the levels of FSH and LH, as well as an abnormality in the levels of oxidative stress markers MDA and SOD by ELISA (Fig. 7A-G). Furthermore, the results of qRT-PCR and WB revealed that the increased expression of VEGF, VEGFR-2, FAK, p-VEGFR-2 and p-FAK induced by YJD in TP-induced KGN cells was reversed by the addition of Avastin, SU5408 or Y15 (Fig. 7H-L). Similarly, the inhibited apoptosis and reduced expression of

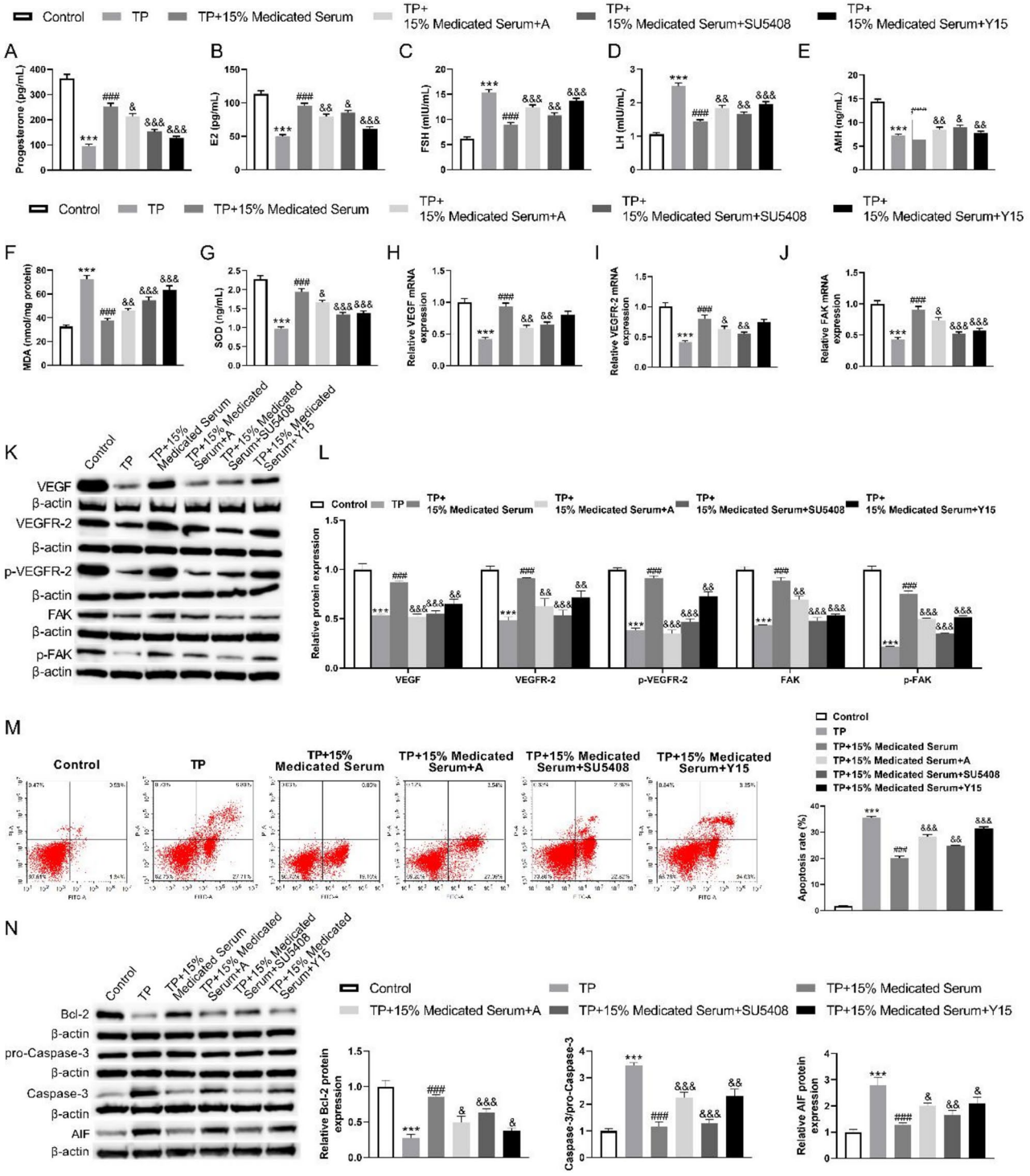

Fig. 7 YJD affected POF by regulating the VEGF/VEGFR-2/FAK signaling pathway. (**A**–**E**) Serum levels of the hormones P, E2, FSH, LH, and AMH were examined by ELISA. Control and TP groups were set up, and the remaining groups were co-treated with TP and 15% medicated serum, along with VEGF inhibitor (Avastin), VEGFR-2 inhibitor (SU5408), or FAK inhibitor (Y15). (**F**-**G**) Serum levels of indicators of oxidative stress, MDA and SOD were assessed by ELISA. (**H**-**J**) The expression of VEGF, VEGFR-2, and FAK was detected by qRT-PCR. (**K**-**L**) The expression of VEGF, VEGFR-2, FAK, p-VEGFR-2 and p-FAK were assessed by WB. (**M**) Apoptosis rate was detected by Annexin V-FITC flow cytometry. (**N**) The expression of Bcl-2, pro-Caspase-3, Caspase-3 and AIF were assessed by western blotting. $^{**}P < 0.01$, $^{***}P < 0.001$ vs. Control; $^{\#\#}P < 0.01$, $^{\#\#\#}P < 0.001$ vs. TP; $^{\&}P < 0.05$, $^{\&\&}P < 0.01$, $^{\&\&\&}P < 0.001$ vs. TP + 15% medicated serum

Table 2 Pregnancy rate, number of implanted embryos, number of live births, and body weight of newborn rats

Group	Pregnancy rate (%)	Average number of implantation sites	Number of live births	Body weight of newborn rats (g)
Control	90.00% (9/10)	16.67 ± 0.58	15.67 ± 1.22	7.62 ± 0.14
TP	42.86% (3/7)	9.33 ± 1.53***	9.33 ± 1.53***	6.87 ± 0.25***
TP + L-YJD	50.00% (4/8)	12.33 ± 0.58	12.00 ± 0.41$^{\#\#\#}$	7.00 ± 0.17$^{\#\#}$
TP + M-YJD	62.50% (5/8)	14.00 ± 0.00$^{\#\#}$	12.40 ± 1.14$^{\#\#\#}$	7.31 ± 0.16$^{\#\#\#}$
TP + H-YJD	57.14% (4/7)	12.33 ± 0.58$^{\#}$	11.75 ± 0.96$^{\#\#}$	7.01 ± 0.25$^{\#}$
TP + DHEA	77.78% (7/9)	15.00 ± 1.00$^{\#\#\#}$	14.71 ± 1.38$^{\#\#\#\&}$	7.41 ± 0.20$^{\#\#\#\&\&}$

$^{*}P<0.05$, $^{**}P<0.01$, $^{***}P<0.001$ vs. Control; $^{\#}P<0.05$, $^{\#\#}P<0.01$, $^{\#\#\#}P<0.001$ vs. TP; $^{\&}P<0.05$, $^{\&\&}P<0.01$, $^{\&\&\&}P<0.001$ vs. TP + M-YJD

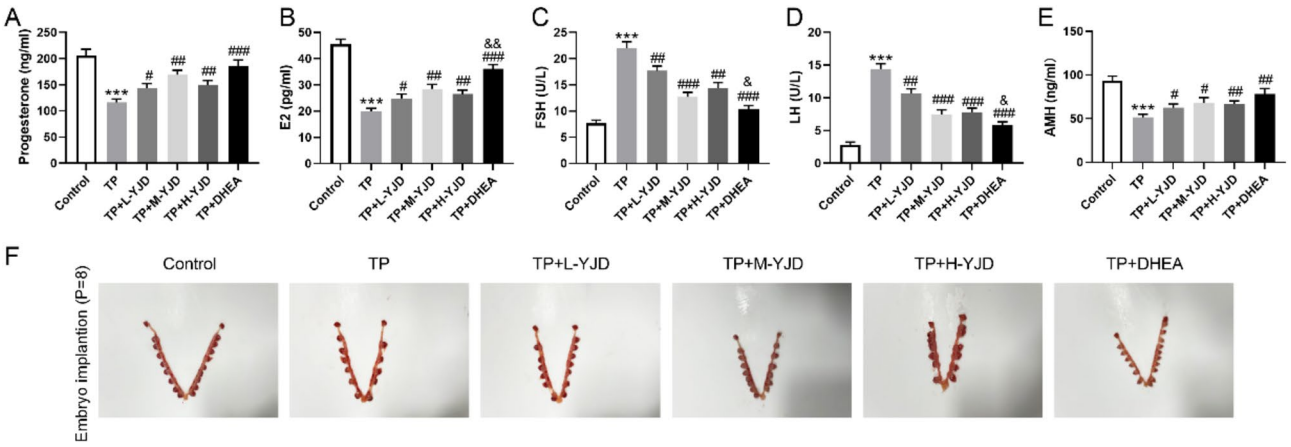

Fig. 8 Effect of YJD on fertility in rats with POF. (**A**–**E**) The levels of serum hormones P, E2, FSH, LH and AMH in rats were assessed by ELISA. After rats were modeled with TP, L-YJD, M-YJD and H-YJD as well as DHEA positive controls were administrated to POF rats. (**F**) Representative images of the uterus of pregnant rats. $^{***}P<0.001$ vs. Control; $^{\#}P<0.05$, $^{\#\#}P<0.01$, $^{\#\#\#}P<0.001$ vs. TP; $^{\&}P<0.05$, $^{\&\&}P<0.01$, $^{\&\&\&}P<0.001$ vs. TP + M-YJD

apoptotic factors in TP-induced KGN cells by YJD were also altered by the addition of Avastin, SU5408 or Y15 via flow cytometry and WB (Fig. 7M-N). These findings presented above indicated that YJD induced normalization of sex hormone and oxidative stress levels, as well as promoted angiogenesis in TP-induced KGN cell models. However, the effect of YJD on TP-induced KGN cell models was reversed by angiogenesis inhibitors. Therefore, YJD improved TP-induced KGN cell function and reduced oxidative stress levels through the activation of the VEGF/VEGFR-2/FAK signaling pathway.

YJD improved the fertility of pregnant POF rats

In order to investigate the impact of YJD on the fertility of POF rats, an analysis was conducted on the pregnancy rate, number of implanted embryos, number of live births, and weight of newborn rats in each group, as detailed in Table 2. Both YJD and DHEA treatments resulted in an increase in the pregnancy rate, number of implanted embryos, number of live births, and body weight of newborn rats in POF rats. Furthermore, the ELISA assays revealed a significant decrease in the levels of P, E2, and AMH in pregnant rats with POF, along with a significant increase in FSH and LH. Additionally, treatment with YJD was found to improve the sex hormone levels in pregnant POF rats, with the best effect in M-YJD treatment (Fig. 8A-E). Moreover, the uterine embryo landing plots of different groups of pregnant mice were shown in Fig. 8F. YJD and DHEA group embryos were uniformly sized, fully developed, and had no blood in the uterus, while model group embryos were unevenly distributed, small, and irregularly shaped with some blood in the uterus. In summary, YJD improved sex hormone levels and ovarian function in pregnant POF rats and improved their reproductive capacity.

Discussion

POF is one of the most serious diseases affecting women's reproductive health in the current era. Although there are various causes of POF, such as genetic abnormalities, autoimmune factors, medical factors, infectious factors, toxins, and environmental factors, in most cases, the cause of POF cannot be identified after a comprehensive evaluation [22]. With the increasing incidence of cancer, radiotherapy and chemotherapy are gradually becoming the main cause of POF in young women [23]. This not only affects women's fertility, but also seriously influences their mental health and quality of life [24]. This study confirmed that YJD improved POF symptoms by ameliorating oxidative stress damage and promoting angiogenesis, which provided a direction for clinical treatment to improve ovarian function.

TP is an active compound extracted from the Chinese herb Lei Gong Teng [25]. It has been shown to possess anti-inflammatory, immunosuppressive and anticancer activities. However, the use and development of TP has been extremely limited because it causes serious damage to the liver, kidneys and reproductive system [26]. Oxidative stress is the predominant mechanism of TP-induced injury [27]. TP and its toxic metabolites interfere with the intracellular antioxidant system and impair its detoxification. This may eventually lead to oocyte degeneration, granulosa cell apoptosis and impaired hormone secretion [28]. Furthermore, it has also been shown that excessive oxidative stress damage has a detrimental effect on angiogenesis. SOD is an important enzyme in the antioxidant defense process and plays an important role in protecting cells and tissues [29]. MDA is a major metabolite of lipid peroxidation and an important marker of oxidative stress damage [30]. The present study utilized TP to induce POF models in rats and KGN cells. The observed decrease in SOD levels and increase in MDA accumulation in the TP-induced model resulted in localized oxidative damage within the ovary, aligning with findings from previous research. Moreover, treatment with YJD demonstrated an ameliorative effect on TP-induced oxidative stress levels.

The rodent estrous cycle is characterized by morphological changes in the ovaries, uterus, and vagina, making it a valuable metric for monitoring reproductive performance [31]. The estrous cycle in female rats typically lasts from 4 to 5 days [32]. Although there might be potential delays or advances in specific phases of the estrous cycle in the rat models in the course of this study, resulting in irregularity of the estrous cycle. However, it had no remarkable impact on the results of the study. These findings confirmed that YJD improved ovarian dysfunction in TP-induced POF rats by restoring the normal estrous cycle and facilitating ovarian size normalization. Moreover, MVH and Oct4 are often used as molecular markers of germ cells [33, 34]. In the POF rat models, treatment with YJD restored the TP-induced reduction in MVH and Oct4 expression. On the other hand, sex hormone levels are closely related to ovarian function. AMH inhibits the development of male mullerian ducts and regulates the development of reproductive cells and gonads in both sexes [35, 36]. It can be used as an indicator to evaluate the ovarian reserve function. In addition, E2 is a naturally occurring estrogen that is integral to the preservation of female secondary sexual characteristics. The expression of P and E2 has been linked to follicular growth [37]. FSH is primarily produced by the basophilic cells of the pituitary gland. Working in conjunction with LH, FSH facilitates the maturation of follicles, leading to the secretion of P and estrogen [38, 39]. Our experimental data showed that YJD increased E2, P, and AMH levels as well as reduced FSH and LH levels, improving ovarian function and fertility in POF rats during diestrus and pregnancy.

The process of angiogenesis in the ovary is intricate, involving both neovascularization and vascular maturation [40]. Key cell types implicated in this process are vascular endothelial cells and pericytes [41]. Vascular endothelial cells proliferate and migrate to establish neovascularization, while pericytes play a crucial role in ensuring vascular integrity and stabilization through their recruitment [42]. The collaboration between vascular endothelial cells and pericytes is vital for microvascular remodeling and stabilization [43]. In the present investigation, vascular endothelial cells and pericytes were identified using CD31 and α-SMA markers, respectively. Findings revealed a notable elevation in CD31 and α-SMA positive staining within the follicle and corpus luteum following YJD treatment as opposed to the TP-induced model group. These results indicated that YJD mitigated vascular damage in the ovaries of POF rats by enhancing angiogenesis and promoting vascular stability. Furthermore, the angiogenic process necessitates the collaborative involvement of multiple essential factors. VEGF is a major factor involved in cell proliferation, migration, survival and vascular permeability of vascular endothelial cells [44]. The pro-angiogenic effect of VEGF is mediated by binding to VEGFR-2, which triggers a series of intracellular signaling channels. FAK is a downstream signal effector of VEGF/ VEGFR-2 pathway, which is closely related to cell adhesion, diffusion, proliferation, migration and apoptosis [45]. In both POF rat and KGN cell models, YJD demonstrated a significant enhancement in the expression levels of VEGF, VEGFR-2, and FAK, ultimately facilitating ovarian angiogenesis. In addition, VEGF/VEGFR-2/FAK inhibitors were found to reverse the effect of YJD in TP-induced KGN cells. Consequently, the modulation of the VEGF/VEGFR-2/FAK signaling pathway by YJD appeared to be a promising therapeutic approach for improving POF.

Caspase-3 is at the center of the caspase cascade reaction and is a common pathway for all apoptotic signaling pathway [46]. Bcl-2 and Caspase-3 interact with each other to regulate the process of apoptosis. In this work, the treatment of YJD significantly decreased the expression of Caspase-3 and AIF, while the expression of Bcl-2 was significantly increased. The effect of YJD on apoptosis in the treatment of POF deserved further exploration.

Several recent studies have indicated that maternal exposure to TP to conception may impact pregnancy outcomes and result in long-term negative consequences for future generations [47]. Our study revealed notable decrease in pregnancy rates, reduction in the number of implanted embryos and severe uterine hemorrhaging in the TP-induced model group. Conversely, the group

treated with YJD did not exhibit uterine hemorrhaging and displayed a more uniform distribution of embryos. The findings of this study indicated that M-YJD had a significant impact on both the pregnancy rate and the number of embryos implanted, suggesting its potential to enhance the intrauterine microenvironment for successful implantation and subsequent live births. Further comprehensive research is needed to fully understand the mechanisms by which YJD may influence in utero embryo development. In the present research, the therapeutic effects of YJD at the selected dose gradients on POF rats did not exhibit a dose-dependent response. This phenomenon may be attributed to the complexity of the herbal formula components, the multi-target synergistic effects, and the feedback regulation mechanisms of the body [48]. The pharmacological effects of the various components in the herbal formula may be either synergistic or antagonistic [49]. Additionally, the current dose gradient of YJD used in this work may not fully cover the critical nodes of the "dose-response" curve, which could explain the absence of a dose-dependent effect. In future studies, it would be beneficial to further explore the optimal dose range of YJD by incorporating pharmacokinetic analyses and to comprehensively evaluate the overall effects of the herbal formula using multi-omics approaches, which will enhance the potential of YJD in the treatment of POF.

Conclusion

In conclusion, the administration of YJD resulted in a significant improvement in sex hormone levels and ovarian function in rats with POF. Furthermore, YJD demonstrated a protective effect on ovarian tissue by alleviating oxidative damage through enhancing SOD levels and reducing MDA accumulation, as well as promoting angiogenesis through the regulation of the VEGF/VEGFR-2/FAK signaling pathway. Additionally, YJD was found to enhance the intrauterine implantation microenvironment, leading to an increase in pregnancy rates and live birth numbers.

Abbreviations

AMH	Anti-mullerian hormone
CD31	Platelet endothelial cell adhesion molecule-1
DHEA	Dehydroepiandrosterone
E2	Estradiol
ELISA	Enzyme-linked immunosorbent assay
ETCM	Encyclopedia of traditional Chinese medicine
FITC	Fluorescein isothiocyanate
FSH	Follicle stimulating hormone
GEO	Gene expression omnibus
GO	Gene ontology
HE	Staining of hematoxylin and eosin
KEGG	Kyoto encyclopedia of genes and genomes
LH	Luteinizing hormone
MDA	Malondialdehyde
OMIM	Online mendelian inheritance in humans
P	Progesterone
PBS	Phosphate buffer solution
PI	Propidium iodide
POF	Premature varian failure
PPI	Protein-protein interaction
PMSG	Pregnant Mare Serum Gonadotropin
qRT-PCR	Quantitative real-time PCR
ROS	Reactive oxygen species
SD	Sprague Dawley
SOD	Superoxide dismutase
TCM	Traditional Chinese medicine
TCMSP	Traditional Chinese medicine systematic pharmacology
TP	Triptolide
YJD	Yijing decoction
α-SMA	α-Smooth muscle actin

Supplementary Information

The online version contains supplementary material available at https://doi.org/10.1186/s13048-025-01679-2.

Supplementary Material 1

Acknowledgements

The authors thank all colleagues and support from Henan Provincial People's Hospital.

Author contributions

RG: Conceptualization, Data curation, Formal analysis, Investigation, Writing-original draft, Writing-review & editing. YW: Conceptualization, Data curation, Formal analysis, Investigation, Writing-original draft, Writing-review & editing. YT: Formal analysis, Software, Methodology, Writing-original draft, Writing-review & editing. KW: Software, Methodology, Writing-review & editing. BG: Conceptualization, Funding acquisition, Project administration, Resources, Supervision, Writing-review & editing.

Funding

The present study was supported by the National Natural Science Foundation of China (Grant No. 81873334 and 81973684), the Natural Science Foundation of Sichuan Province (Grant No. 2023NSFSC1760) and Henan Province Postdoctoral Research Program (Grant No. HN2024079), and Health Commission of Chengdu and Chengdu University of Traditional Chinese Medicine Joint Innovation Fund in 2024 (Grant No. WXLH202402019).

Data availability

The datasets generated and/or analysed during the current study are not publicly available due [REASON WHY DATA ARE NOT PUBLIC] but are available from the corresponding author on reasonable request.

Declarations

Ethics approval and consent to participate

All animal experimental procedures were performed in accordance with the Institutional Animal Care and Use Committee of Henan Provincial People's Hospital, which was approved by the Institutional Animal Care and Use Committee of Henan Academy of Traditional Chinese Medicine Animal Experiment Center (SYXK (Yu) 2022-0007).

Patient consent for publication

Not applicable.

Competing interests

The authors declare no competing interests.

Received: 19 November 2024 / Accepted: 21 April 2025
Published online: 26 April 2025

References

1. Ghahremani-Nasab M, et al. Premature ovarian failure and tissue engineering. J Cell Physiol. 2020;235(5):4217–26.
2. Liu M, et al. MicroRNA-144-3p protects against chemotherapy-induced apoptosis of ovarian granulosa cells and activation of primordial follicles by targeting MAP3K9. Eur J Med Res. 2023;28(1):264.
3. Deady J. Clinical monograph: hormone replacement therapy. J Managed Care Pharmacy: JMCP. 2004;10(1):33–47.
4. Wang Y, Teng X, Liu J. Research progress on the effect of traditional Chinese medicine on signal pathway related to premature ovarian insufficiency. Evidence-based Complement Altern Medicine: eCAM. 2022;2022:p7012978.
5. Yan J, et al. [Effects of Rehmanniae Radix and Rehmanniae Radix Praeparata on proteomics and autophagy in mice with type 2 diabetes mellitus induced by high-fat diet coupled with streptozotocin]. Zhongguo Zhong yao za zhi = Zhongguo zhongyao zazhi = China. J Chin Materia Med. 2023;48(6):1535–45.
6. Zhou W, et al. Comprehensive quality evaluation of two different geography originated Angelica sinensis Radix based on potential production area development and resource protection. Volume 201. Plant physiology and biochemistry: PPB; 2023. p. 107878.
7. Chen C, et al. Radix paeoniae Alba attenuates Radix Bupleuri-induced hepatotoxicity by modulating gut microbiota to alleviate the Inhibition of saikosaponins on glutathione synthetase. J Pharm Anal. 2023;13(6):640–59.
8. Jeong J, et al. Triple herbal extract DA-9805 exerts a neuroprotective effect via amelioration of mitochondrial damage in experimental models of Parkinson's disease. Sci Rep. 2018;8(1):15953.
9. Hu P, et al. An UPLC-MS/MS method for targeted analysis of microbial and host Tryptophan metabolism after administration of polysaccharides from atractylodes macrocephala Koidz. In ulcerative colitis mice. J Pharm Biomed Anal. 2023;235:115585.
10. Zhang X, et al. First report of root rot caused by fusarium Armeniacum on American ginseng in China. Plant Dis. 2020;105(4):1223.
11. Ji Q, et al. Comparative transcriptome profiling analysis provides insight into the mechanisms for sugar change in Chinese jujube (Ziziphus Jujuba Mill.) under rain-proof cultivation. Plant Genome. 2023;16(2):e20341.
12. Xue-Han LJ-JHG-RL. Clinical study of modified Yijing Decoction combined with artificial periodic therapy for the treatment of diminished ovarian reservation. J Guangzhou Univ Traditional Chin Med. 2022;39(9):2021–7.
13. Shimizu T. Molecular and cellular mechanisms for the regulation of ovarian follicular function in cows. J Reprod Dev. 2016;62(4):323–9.
14. Qiao J, Feng H. Extra- and intra-ovarian factors in polycystic ovary syndrome: impact on oocyte maturation and embryo developmental competence. Hum Reprod Update. 2011;17(1):17–33.
15. Robinson R, et al. Angiogenesis and vascular function in the ovary. Reprod (Cambridge England). 2009;138(6):869–81.
16. Nie X, et al. Establishment of a mouse model of premature ovarian failure using consecutive superovulation. Cell Physiol Biochemistry: Int J Experimental Cell Physiol Biochem Pharmacol. 2018;51(5):2341–58.
17. Moldogazieva N, et al. Oxidative stress and advanced lipoxidation and glycation end products (ALEs and AGEs) in aging and Age-Related diseases. Oxidative Med Cell Longev. 2019;2019:p3085756.
18. Schallreuter K, et al. In vivo and in vitro evidence for hydrogen peroxide (H2O2) accumulation in the epidermis of patients with vitiligo and its successful removal by a UVB-activated pseudocatalase. J Invest Dermatology Symp Proc. 1999;4(1):91–6.
19. Kashino G, et al. VEGF affects mitochondrial ROS generation in glioma cells and acts as a radioresistance factor. Radiat Environ Biophys. 2023;62(2):213–20.
20. Limei L, et al. Effect of modified Yijing Decoction on sex hormones and ovarian histomorphology in rats with ovarian hypofunction. Chin Med Rev. 2021;27(02):24–6.
21. Zhou F, et al. Si-Wu-Tang facilitates ovarian function through improving ovarian microenvironment and angiogenesis in a mouse model of premature ovarian failure. J Ethnopharmacol. 2021;280:114431.
22. Ebrahimi M, Akbari F, Asbagh. Pathogenesis and causes of premature ovarian failure: an update. Int J Fertility Steril. 2011;5(2):54–65.
23. Rodriguez-Wallberg K, Oktay K. Options on fertility preservation in female cancer patients. Cancer Treat Rev. 2012;38(5):354–61.
24. Howard-Anderson J, et al. Quality of life, fertility concerns, and behavioral health outcomes in younger breast cancer survivors: a systematic review. J Natl Cancer Inst. 2012;104(5):386–405.
25. Gao H, et al. Triptolide induces autophagy and apoptosis through ERK activation in human breast cancer MCF-7 cells. Experimental Therapeutic Med. 2018;15(4):3413–9.
26. Deng Y, et al. Triptolide sensitizes breast cancer cells to doxorubicin through the DNA damage response Inhibition. Mol Carcinog. 2018;57(6):807–14.
27. Zhao F, et al. Triptolide induces protective autophagy through activation of the CaMKKβ-AMPK signaling pathway in prostate cancer cells. Oncotarget. 2016;7(5):5366–82.
28. Vliegenthart A, et al. Characterization of Triptolide-Induced hepatotoxicity by imaging and transcriptomics in a novel zebrafish model. Toxicol Sci. 2017;159(2):380–91.
29. Fu K, et al. Xanthotoxin induced photoactivated toxicity, oxidative stress and cellular apoptosis in Caenorhabditis elegans under ultraviolet A. Comp Biochem Physiol C Toxicol Pharmacol. 2022;251:109217.
30. Ramachandran A. H. Jaeschke 2019 Acetaminophen hepatotoxicity: A mitochondrial perspective. Adv Pharmacol (San Diego Calif) 85 195–219.
31. Goldman JM, Murr AS, Cooper RL. The rodent estrous cycle: characterization of vaginal cytology and its utility in toxicological studies. Birth Defects Res B Dev Reprod Toxicol. 2007;80(2):84–97.
32. Cora MC, Kooistra L, Travlos G. Vaginal cytology of the laboratory rat and mouse: review and criteria for the staging of the estrous cycle using stained vaginal smears. Toxicol Pathol. 2015;43(6):776–93.
33. Nagamori I, Cruickshank V, Sassone-Corsi P. Regulation of an RNA granule during spermatogenesis: acetylation of MVH in the chromatoid body of germ cells. J Cell Sci. 2011;124:4346–55.
34. Morrison G, Brickman J. Conserved roles for Oct4 homologues in maintaining multipotency during early vertebrate development. Development. 2006;133(10):2011–22.
35. Boucret L, et al. Relationship between diminished ovarian reserve and mitochondrial biogenesis in cumulus cells. Hum Reprod (Oxford England). 2015;30(7):1653–64.
36. Lunding S, et al. AMH as predictor of premature ovarian insufficiency: A longitudinal study of 120 Turner syndrome patients. J Clin Endocrinol Metab. 2015;100(7):E1030–8.
37. Komatsu K, Masubuchi S. The concentration-dependent effect of progesterone on follicle growth in the mouse ovary. J Reprod Dev. 2017;63(3):271–7.
38. Bosch E, et al. Reduced FSH and LH action: implications for medically assisted reproduction. Hum Reprod (Oxford England). 2021;36(6):1469–80.
39. Moolhuijsen L, Visser J. Anti-Müllerian hormone and ovarian reserve: update on assessing ovarian function. J Clin Endocrinol Metab. 2020;105(11):3361–73.
40. Gaengel K, et al. Endothelial-mural cell signaling in vascular development and angiogenesis. Arterioscler Thromb Vasc Biol. 2009;29(5):630–8.
41. Herbert S, Stainier D. Molecular control of endothelial cell behaviour during blood vessel morphogenesis. Nat Rev Mol Cell Biol. 2011;12(9):551–64.
42. Sugino N, et al. Angiogenesis in the human corpus luteum. Reproductive Med Biology. 2008;7(2):91–103.
43. Davis GE, Norden PR, Bowers SL. Molecular control of capillary morphogenesis and maturation by recognition and remodeling of the extracellular matrix: functional roles of endothelial cells and pericytes in health and disease. Connect Tissue Res. 2015;56(5):392–402.
44. Apte R, Chen D, Ferrara N. VEGF in signaling and disease: beyond discovery and development. Cell. 2019;176(6):1248–64.
45. Claesson-Welsh L, Welsh M. VEGFA and tumour angiogenesis. J Intern Med. 2013;273(2):114–27.
46. Hadji A, et al. Caspase-3 triggers a TPCK-sensitive protease pathway leading to degradation of the BH3-only protein puma. Apoptosis: Int J Program Cell Death. 2010;15(12):1529–39.
47. Wen X, et al. A systematic review and Meta-Analysis of the inhibitory effects of Plant-Derived sterilants on rodent population abundance. Toxins (Basel). 2022;14(7).
48. Li C, et al. Traditional Chinese medicine in depression treatment: from molecules to systems. Front Pharmacol. 2020;11:586.
49. Ung CY, et al. Are herb-pairs of traditional Chinese medicine distinguishable from others? Pattern analysis and artificial intelligence classification study of traditionally defined herbal properties. J Ethnopharmacol. 2007;111(2):371–7.

Publisher's note